European Journal of Medicinal Chemistry 158 (2018) 733–742

Contents lists available at ScienceDirect

European Journal of Medicinal Chemistry

journal homepage: http://www.elsevier.com/locate/ejmech

Research paper

# Conformation impacts on the bioactivities of SMART analogues

Yue Wu [a], Qi Guan [a], Dayong Zheng [b], Peng Yan [a], Dongjie Feng [a], Jianan Du [b], Jingbo Zhang [a], Daiying Zuo [b, ***], Kai Bao [a, c, **], Weige Zhang [a, *]

[a] Key Laboratory of Structure-Based Drug Design and Discovery, Ministry of Education, Shenyang Pharmaceutical University, 103 Wenhua Road, Shenhe District, Shenyang, 110016, China
[b] Department of Pharmacology, Shenyang Pharmaceutical University, 103 Wenhua Road, Shenhe District, Shenyang, 110016, China
[c] Wuya College of Innovation, Shenyang Pharmaceutical University, 103 Wenhua Road, Shenhe District, Shenyang, 110016, China

ARTICLE INFO

*Article history:*
Received 29 April 2018
Received in revised form
13 August 2018
Accepted 14 September 2018
Available online 15 September 2018

*Keywords:*
Tubulin
CBSI
Conformation
Molecular modeling
DFT

ABSTRACT

As promising colchicine binding site inhibitors, SMART and its analogues have attracted many research efforts in recent years. A large number of SMART analogues with different B-rings have been reported; however, the effects of B-ring on the bioactivity are still unclear so far. Herein, we speculated that the conformational preference caused by B-rings was crucial for active SMART analogues. Our assumption was supported by the molecular docking studies, molecular dynamic simulation and DFT computations of SMART and its analogues reported by other and our research groups. Moreover, several novel SMART analogues with different conformational preferences were designed and synthesized to disclose the conformation impacts, and the preliminary biological evaluation was in accordance with our assumption.


## 1. Introduction

Microtubules are protein biopolymers formed through polymerization of heterodimers of α- and β-tubulin [1]. The polymerization dynamics of tubulin relates to a number of cell functions including mitosis. Thus tubulin is a promising target for new chemotherapeutic agents since cancer cells undergo mitosis at a significantly increased rate [2]. As the first tubulin depolymerizing agent, colchicine inhibits polymerization of tubulin by a steric clash between α- and β-tubulin. Although colchicine (1, Fig. 1) is not used as an anticancer agent due to its low therapeutic index, its binding site still attracts many attentions [3]. Over decades, a large number of colchicine binding site inhibitors (CBSIs) have been reported. Among them, agents with 3,4,5-trimethoxyphenyl (TMP) moiety (**2**–**4**, **4** possesses a semi-TMP moiety) represent an important class of CBSIs. Structure-activity relationship (SAR) indicates that all three methoxy groups are necessary for high potency. Crystal structures of these compounds in complex with tubulin dimer proved that TMP (or semi-TMP) moiety is located in domain II of colchicine binding site, and one methoxy group could contribute a hydrogen bond with β-CYS241 [4].

4-Substituted methoxybenzoyl-aryl-thiazole (SMART, **5**, Fig. 2) [5] could strongly inhibit tubulin polymerization through binding to the colchicine site of tubulin and significantly enhance the growth inhibition against a variety of cancer cells, including multidrug resistant cancer cell lines. Previous studies have yielded a series of chemically diverse SMART analogues (**6~25**) [6–17] that generally have a three-ring scaffold (A, B and C conjugated aromatic rings) with a carbonyl group between A- and B-ring. SAR of SMART analogues revealed that TMP moiety as A-ring is crucial for optimal activity. As for C-ring, there is no specific requirement for substitution, but *p*-methylphenyl or nonsubstituted rings are preferred [18]. Modifications of B-ring are generally tolerated for SMART analogues and the thiazole ring of **5** could be replaced with other heteroaromatic rings.

The effects of different B-rings have not acquired enough attention yet, as most of the previous studies focus on a series of analogues with a particular B-ring. As shown in Figs. 2, **21~25** show low antiproliferative activity (>10 μM), in spite of their structures that are similar to other SMART analogues [15–17]. **5** and **23** both

* Corresponding author.
** Corresponding author. Key Laboratory of Structure-Based Drug Design and Discovery, Ministry of Education, Shenyang Pharmaceutical University, 103 Wenhua Road, Shenhe District, Shenyang, 110016, China.
*** Corresponding author.
*E-mail addresses:* zuodaiying@163.com (D. Zuo), kbao@syphu.edu.cn (K. Bao), zhangweige@syphu.edu.cn (W. Zhang).

https://doi.org/10.1016/j.ejmech.2018.09.045
0223-5234/

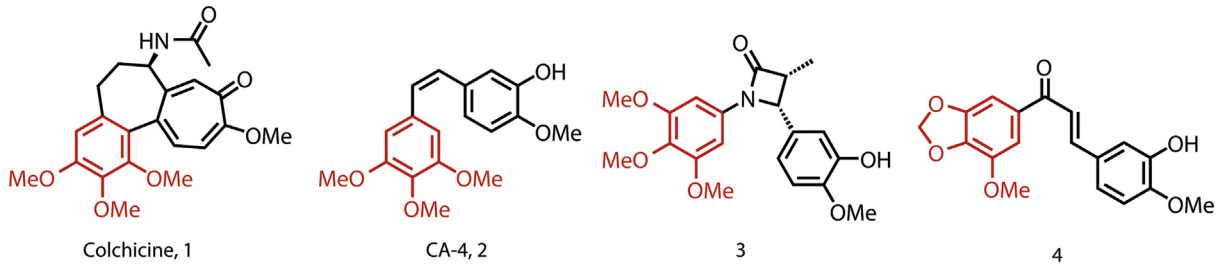


**Fig. 1.** Structures of reported CBSIs.

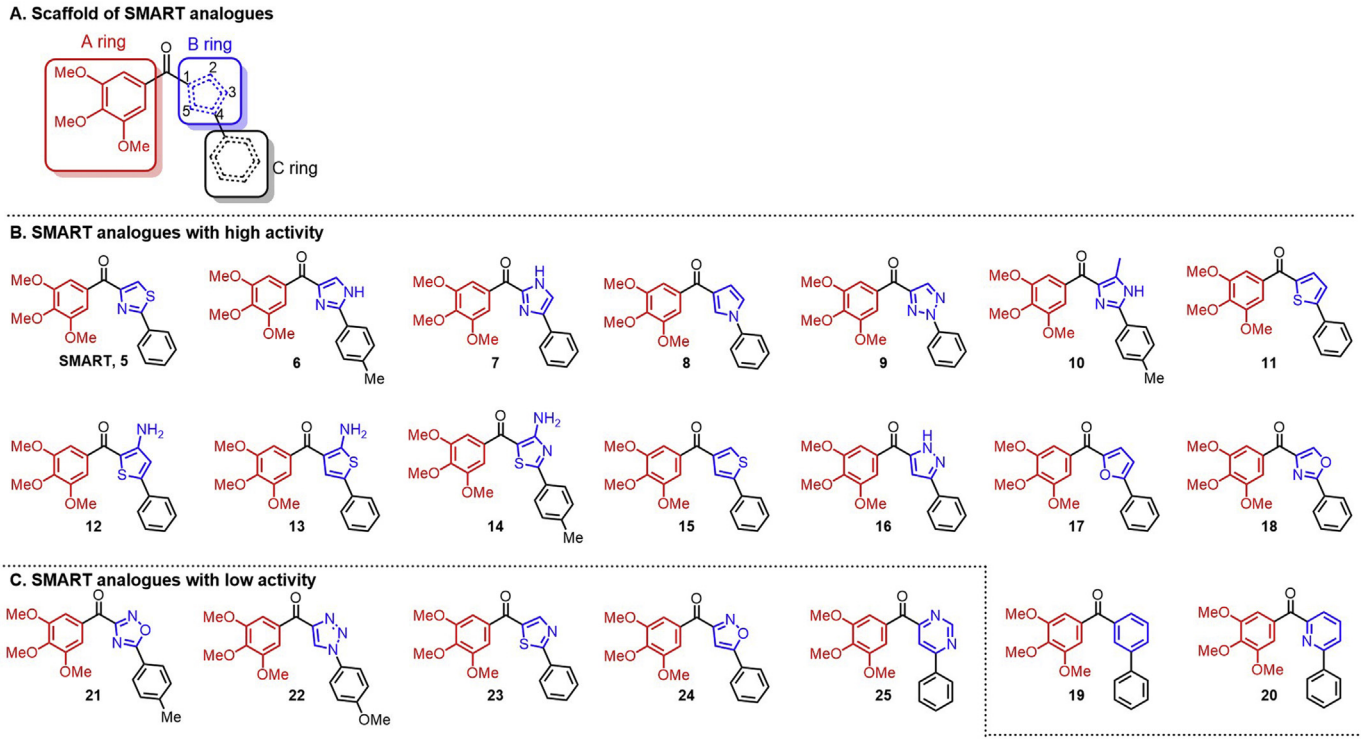


**Fig. 2.** Structures of SMART analogues.

have a thiazole B-ring [5]; however, **5** shows nanomoles level activity and **23** has no activity against several cancer cell lines [15]. Miller et al. investigated the effects of different B-rings (**15**~**20**, **23**~**25**) [15] and obtained some interesting SAR results. A further systematic study is still necessary for the insightful understanding of the role of B-ring.

Conformational isomerism plays a key role in the activity of drug molecules and is an important consideration for rational drug design. In the absence of a co-crystal structure of SMART analogues complex with tubulin dimer, the determination of the ligands conformation at the binding site is challenging. To date, no binding mode has been proposed to satisfy all SMART analogues and detail the role of B-ring. On the other hand, because of the rotatable bond between the carbonyl group and B-ring, SMART analogues have two relatively stable conformations, "straight" and "bent" (Fig. 3). Both of them were considered as possible binding conformations by independent studies [6–11,13,14,16]. In the present work, we aimed to establish a binding mode for all SMART analogues and reveal the necessity of B-ring induced "bent" conformation for potency. Moreover, we designed and synthesized several SMART analogues with different conformational preference and compared their bioactivities to support our assumptions.

## 2. Results and discussion

### 2.1. Molecular modeling studies

Previous SAR studies revealed that all three methoxy groups are crucial for the potency of both compound **1**~**4** and SMART analogues. Therefore, we assumed that TMP moiety of SMART analogues should be located in the same domain when binding to the tubulin dimer. Initially, we tried to use the crystal structures of tubulin in complex with colchicine analogues (PDB codes: 1SA0 [19], 3UT5 [20], 4O2B [21] etc.) for molecular docking study. However, it was difficult to find a common mode of these reported crystal structures. To our delight, when crystal structures of tubulin in complex with **2**~**4** (PDB codes: 5LYJ [22], 5GON [23] and 5JVD [24]) were used, the top-ranked docking poses of all SMART analogues in Fig. 2 could be perfectly superposed to the corresponding native ligands (Fig. 4A and C, S1A, and Table S1).

Interestingly, all of the three molecular modeling studies suggested that "bent" conformation is a preferred conformation for

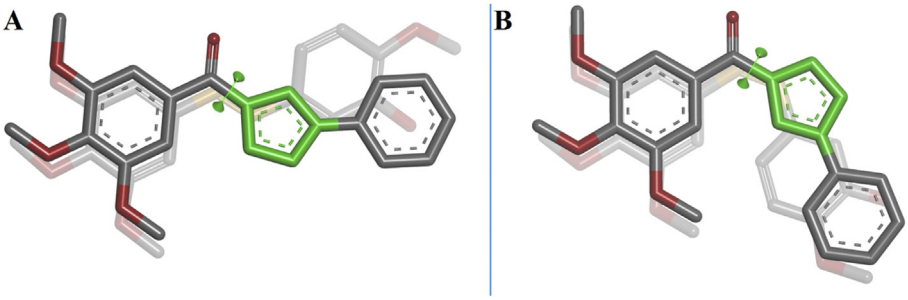


**Fig. 3.** Two relatively stable conformations of SMART and CA-4. **A**. "Straight" conformation of SMART analogues and *trans*-CA-4; **B**. "Bent" conformation of SMART analogues and *cis*-CA-4.

binding. In our binding models, a hydrogen bond between the oxygen of 4-OMe in **5** (also found in all other SMART analogues) and the SH group of β-CYS241 was found in all three crystals (Fig. 4B and D and S1B). Besides, another hydrogen bond could be formed between the carbonyl group of SMART analogues and β-ASN251 in the crystal complex with **4** (Fig. 4D, PDB Code: 5JVD), which could explain the descent of potency when the carbonyl group was substituted [5,7,15].

To further validate the binding mode, a 25-ns molecular dynamic (MD) simulation was carried out for the tubulin (PDB Code: 5LYJ) with a docked pose of **5** and native ligand CA-4, correspondingly. During MD simulation, root mean square deviations (RMSD), the radius of gyration ($R_g$) and root mean square fluctuations (RMSF) were recorded for the purpose of subsequent analysis [25]. RMSDs of all atoms of two binding models have been calculated and shown in Fig. 4E, which indicated that the binding model between **5** and tubulin dimer was as stable as the binding model of between CA-4 and tubulin dimer. The $R_g$ of the backbone atoms of α, β-tubulin in the presence **5** and CA-4 showed similar level of decrease (Fig. 4F), which also showed that stability of the backbone atoms of tubulin dimer was comparable between these two binding models during the MD simulations. The RMSF analysis of α, β-tubulin atoms in the presence of **5** and CA-4 suggested that fluctuations of residues are similar in these two binding models, especially for β-tubulin (Fig. 4G).

It is difficult to make a satisfactory explanation for the effect of B-ring from the scores of molecular docking and physical property like AlogP [26], which is commonly used for logP predication (Table S1). However, it was noticed that all compounds binding with tubulin dimer with a "bent" conformation. Inspired by the binding mode from the complex between tubulin dimer and CA-4, we realized that geometric feature of "bent" SMART analogues was similar to *cis*-CA-4, while "straight" SMART analogues were similar to *trans*-CA-4 (Fig. 3) that was inactive according to previously studies [27]. In addition, Miller et al. reported the crystal structure of compound **5** with "bent" conformation in their study [5]. Thus, we hypothesized that the "bent" conformation may be necessary for the activity of SMART analogues and decided to investigate the relationship between the activity and conformational preference of SMART analogues.

### 2.2. DFT computations and energy comparisons between different conformations

To explain the necessity of "bent" conformation for the bioactivity of SMART analogues, conformational preference of each individual analogue (**5**~**25**) was investigated. The density functional theory (DFT) computations were carried out for the two conformations of each compound. The energy of each conformation was obtained after full optimization (Table 1). We further used thermodynamic equilibrium theory to estimate the proportion of "bent" conformations (the formulas were shown in the *Experimental* section), and its relationships with the reported antiproliferative activities and tubulin assembly activities.

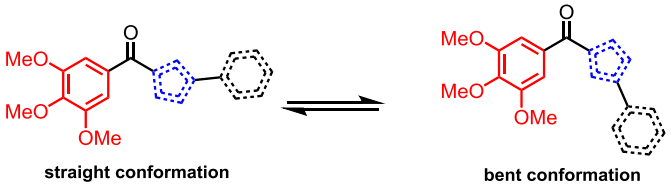


In general, computation study showed that most compounds with high activity have a considerable proportion of "bent" conformation, while compounds with low activity prefer to have less proportion of "bent" conformation (nanomole activity of **5**~**10**, **12**~**14** and **16**~**20** vs micromole or no activity of **21**~**25**). These results obviously displayed the necessity of "bent" conformation for SMART analogues, although we could not establish a quantitative correlativity between the ratio of "bent" conformation and activity. **11** and **15** both have a thiophene B-ring and less than 50% "bent" conformations. The reasons for the high activity of **11** and **15** need more investigation. On the other hand, it was found that **15** shows about 10-fold higher activity than **11**. The proportion of "bent" conformation of **15** was higher than that of **11** (22.2% vs 12.2%), which still indicated the conformation effect of "bent" conformation.

Compared with **11** and **15**, **12** and **13** have an amino group on the 2-position of B-ring, respectively. The molecular modeling studies indicated that the four compounds have a similar binding ability with tubulin dimer (Table S1). However, the proportion of "bent" conformations of **12** and **13** was close to 100% and their activity was increased by 4–20-fold. The high proportion of "bent" conformations of **12** and **13** may be caused by the intramolecular hydrogen bond between the amino and carbonyl group to stabilize the "bent" conformation. On the other hand, the steric hindrance between the amino group and A-ring may destabilize the "straight" conformation of **12** and **13** (Fig. 5 and S2). Similarly, **14** has one more amino group on B-ring than **23** (Fig. S2), and **14** has a much higher proportion of "bent" conformation and a nanomole to sub-nanomole activity (99.8% vs 4.9%, 2–360 nM vs > 10 μM). The effects of the amino group on B-ring may not be limited to its contribution to the proportion of "bent" conformations and needed to be further investigated. However, the computation study clearly showed the relationship between activity and the proportion of "bent" conformation of the SMART analogues.

Previously, we reported that a SMART analogue (**10**) displayed potent cytotoxic activity against various human cancer cells *via* microtubule polymerization inhibition by targeting the colchicine binding site. It is worth mentioning that **10** exhibited comparable

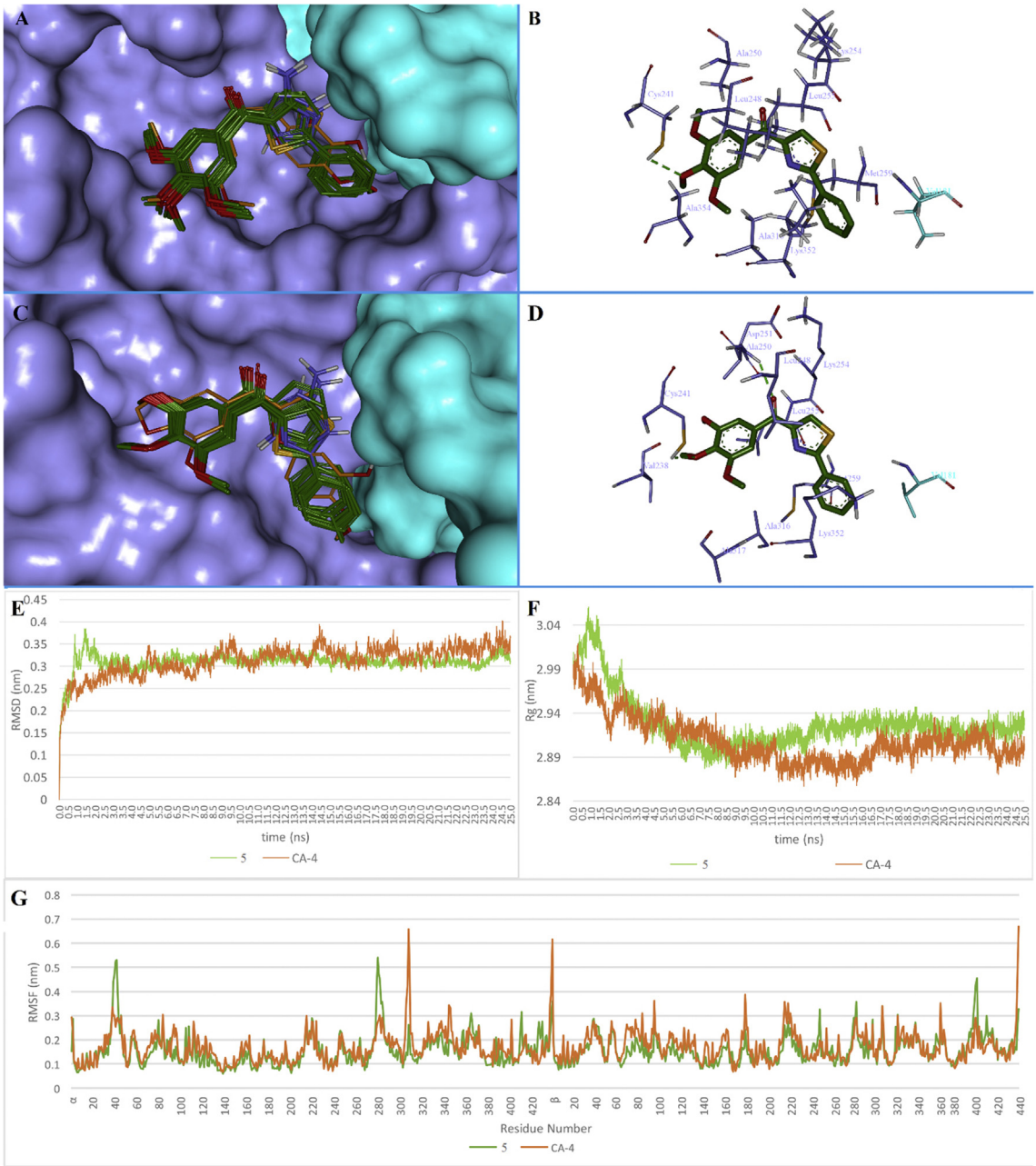


**Fig. 4.** The molecular modeling studies. For molecular docking (**A**~**D**), the color scheme for β-tubulin is lavender, α-tubulin is turquoise, for carbon atoms of SMART analogues and corresponding native ligands are green and orange, respectively. For MD simulation, the color scheme for the curves of binding model of **2** and **5** are green and orange, respectively. **A**. Molecular docking poses of all SMART analogues and **2** in binding pocket (PDB code: 5LYJ); **B**. The interaction between tubulin dimer and **5** (PDB code: 5LYJ); **C**. Molecular docking poses of all SMART analogues and **5** in binding pocket (PDB code: 5JVD); **D**. The interaction between tubulin dimer and **5** (PDB code: 5JVD); **E**. RMSD of all atoms (including tubulin dimer, a $Mg^{2+}$ ion, a GTP molecule and a ligand) of binding models (5LYJ complex with **5** and **2** during 25-ns MD simulation. **F**. $R_g$ of backbone atoms of tubulin dimer of binding models during 25-ns MD simulation; **G**. RMSF of all atoms of tubulin dimer during 25-ns MD simulation. (For interpretation of the references to color in this figure legend, the reader is referred to the Web version of this article.)

or more potency to induce cancer cell death compared to CA-4 and SMART. Computations revealed that the energy difference between **10**'s two conformations was −28.05 kJ/mol and the proportion of "bent" conformation was >99.9%. The methyl group at the 2-position of B-ring of **10** may have contributed to the destabilization of the "straight" conformation of the molecule and caused the high activity of **10**.

In 2014 and 2015, Miller et al. reported a series of potent and metabolically stable tubulin inhibitor, which represented by **26**~**28** [28,29] (Fig. 6). In their continued study, Miller's group investigated the co-crystal structure of **26** complex with tubulin dimer (PDB code: 5H7O [30]) as the first direct evidence of **26**'s direct interaction with the colchicine-binding site in tubulin. **26** could be treated as a SMART analogue carrying the fused heterocyclic scaffold as the bioisosteres of the carbonyl group and B-ring, and 100% proportion of "bent" conformation. To our delight, the molecular modeling studies showed that the top-ranked docking poses of all SMART analogues in Fig. 2 could perfectly be superposed to **26** when 5H7O were used (Figs. S1C and S1D), which suggested that "bent" conformation was a preferred conformation for binding. By

**Table 1**
The binding energy, calculated proportion of "bent" conformation and bioactivity of reported SMART analogues.

| | E("bent")-E("straight") (kJ/mol) | Estimated proportion of "bent" conformation[b] | Antiproliferative activity | Tubulin assembly activity (IC50 ± SD)[a] |
|---|---|---|---|---|
| **5** [5] | −12.89 | 99.4% | 21–71 nM (6 cell lines) | 4.23 μM |
| **6** [6] | −19.10 | >99.9% | 8–46 nM (7 cell lines)<br>10–29 nM (colchicine, 6 cell lines) | N.D. |
| **7** [7] | −36.23 | >99.9% | 5–15 nM (8 cell lines) | N.D. |
| **8** [8] | −0.062 | 50.6% | 20–1300 nM (9 cell lines)<br>13 nM (CA-4) | 1.5 ± 0.2 μM<br>1.0 ± 0.1 μM (CA-4) |
| **9** [9] | −13.78 | 99.6% | 280–700 nM (3 cell lines) | N.D. |
| **10** [10] | −28.05 | >99.9% | 2.4–30.8 nM (15 cell lines) | N.D. |
| **11** [11] | 4.92 | 12.2% | 310–560 nM (5 cell lines) | 1.5 ± 0.1 μM |
| **12** [12] | −24.58 | >99.9% | 4.5–11 nM (4 cell lines)<br>1.6–42 nM (CA-4, 4 cell lines) | 1.2 ± 0.08 μM<br>1.4 ± 0.1 μM (CA-4) |
| **13** [13] | −27.85 | >99.9% | 2.5–3.8 nM (2 cell lines) | 1.3 ± 0.01 μM<br>1.4 ± 0.1 μM (CA-4) |
| **14** [14] | −22.66 | >99.9% | 2–360 nM (6 cell lines)<br>4–3100 nm (CA-4) | 1.6 ± 0.2 μM |
| **15** [15] | 3.12 | 22.2% | 12–72 nM (6 cell lines) | N.D. |
| **16** [15] | −11.92 | 99.2% | 84–245 nM (6 cell lines) | N.D. |
| **17** [15] | −5.42 | 89.8% | 20–151 nM (6 cell lines) | N.D. |
| **18** [15] | −16.17 | 99.8% | 292–600 nM (6 cell lines) | N.D. |
| **19** [15] | −0.66 | 56.5% | 52–500 nM (6 cell lines) | N.D. |
| **20** [15] | −18.62 | 99.9% | 25–39 nM (6 cell lines) | N.D. |
| **21** [16] | 4.34 | 14.9% | >21.5 μM (3 cell lines) | N.D. |
| **22** [17] | 25.09 | <0.1% | No active (no $IC_{50}$ data) | N.D. |
| **23** [15] | 6.38 | 7.2% | >10 μM (6 cell lines) | N.D. |
| **24** [15] | 20.72 | <0.1% | >10 μM (6 cell lines) | N.D. |
| **25** [15] | 16.88 | 0.1% | >20 μM (6 cell lines) | N.D. |

[a] N.D. means no data available.

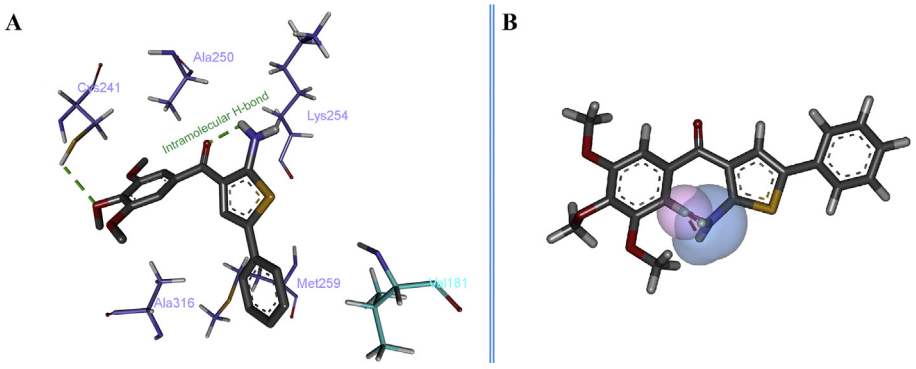


**Fig. 5.** The effect of amino group at 2-position of B-ring. **A**. The interaction between tubulin dimer and **13** (PDB code: 5LYJ). An intramolecular hydrogen bond between the amino group and the carbonyl group in the "bent" conformation. **B**. The steric effect between the amino group and A-ring in the "straight" conformation.

using a similar strategy, we also designed and developed a series of potent SMART analogues carrying the fused heterocyclic scaffold (**29**~**31** [31–33], Fig. 6). This strategy could be considered as an effective approach to keep the absolute "bent" conformations of the molecules.

### 2.3. Molecular design of new SMART analogues

Computations revealed the conformational influences of SMART analogues caused by B-rings. To verify the findings from computations, we designed several novel SMART analogues with different conformational preferences and compared their activity *in vitro*. Three compounds attracted our attention since they were very similar in structure and showed comparable results at the same computational level. The molecular modeling studies indicated that these three compounds have similar binding ability on tubulin dimer (Table S1), while DFT computations suggested that **32** (1,3,4-oxadiazole derivative) and **33** (1,3,4-thiadiazole derivative) had a very small proportion of "bent" conformation (<0.1%), but **34** (1,2,4-triazole derivative) preferred "bent" conformation (>99.9%).

### 2.4. Synthesis

The synthetic routes for all compounds **32**~**34** are outlined in Scheme 1. As the common starting material for **32** and **33**, methyl 3,4,5-trimethoxybenzoate (**35**) was converted into the 2-(3,4,5-trimethoxyphenyl)acetohydrazide (**36**) by hydrazinolysis, followed by acylation with 4-methylbenzoyl chloride to obtain 4-methyl-*N*'-(2-(3,4,5-trimethoxyphenyl)acetyl)benzohydrazide (**37**). Then, different cyclization reactions were carried out for **37** to obtain 1,3,4-oxadiazole core (**38**) [34] or 1,3,4-thiadiazole core (**39**) [35]. For compound **34**, starting material 2-(3,4,5-trimethoxyphenyl)acetonitrile (**40**) was condensed with 4-methylbenzohydrazide under the aid of microwave irradiation to generate 1,2,4-triazole **41** [36]. Finally, **38**, **39** and **41** were oxidized into desired compounds **32**, **33** and **34** by potassium permanganate, respectively.

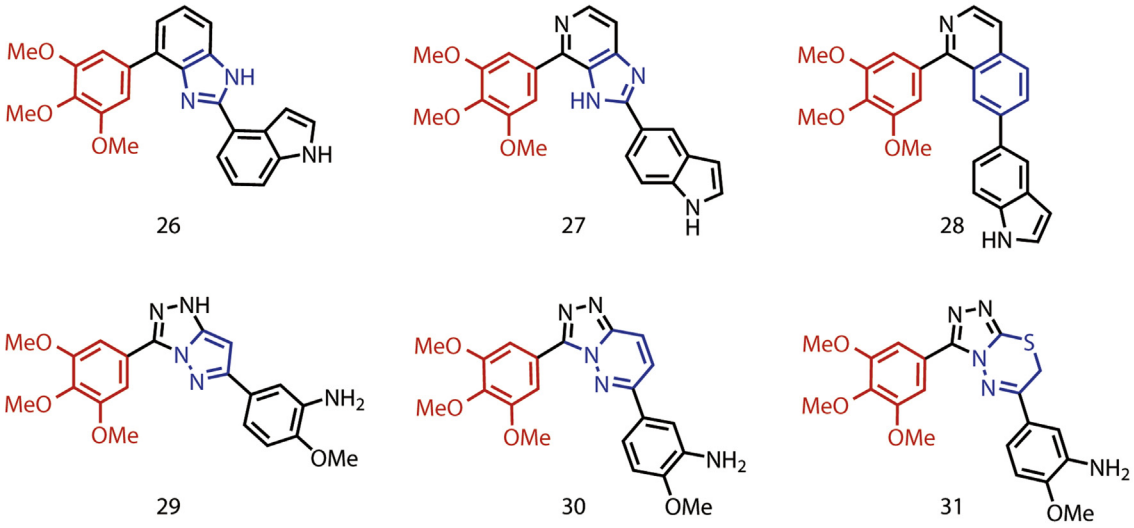


**Fig. 6.** The high potency CBSIs that modified from SMART analogues by fused strategy.

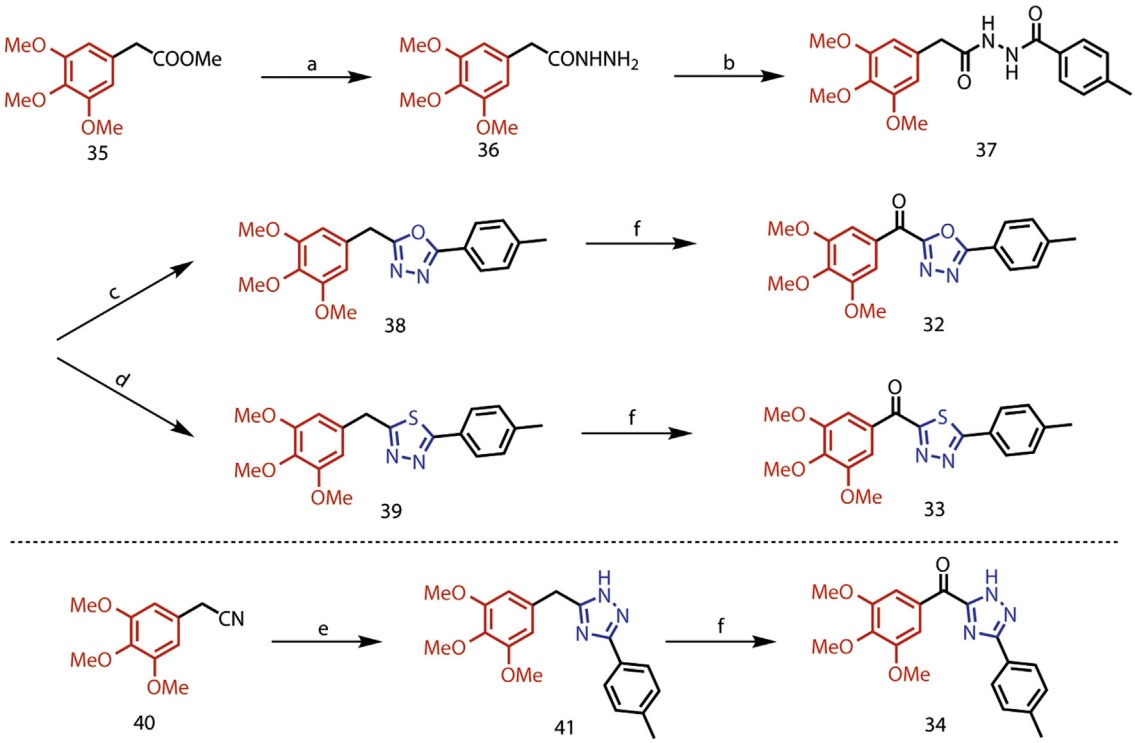


**Scheme 1.** Synthetic route of the designed compounds. Reagents and conditions: (a) $N_2H_4 \cdot H_2O$, methanol, reflux, 2 h; (b) 4-methylbenzoyl chloride, THF, reflux, 2 h; (c) TsCl, $K_2CO_3$, acetone, reflux, 4 h; (d) Lawesson reagent, toluene, reflux, 1 h; (e) 4-methylbenzohydrazide, MW, 150 °C, *n*-BuOH, 25 min; (f) $KMnO_4$, acetone, r.t., 2–6 h.

### 2.5. Biological evaluation

#### 2.5.1. In vitro antiproliferative activity

The synthesized compounds (**32**~**34**) were investigated for their ability to inhibit cancer cells proliferation by the MTT method, using three human carcinoma cell lines: gastric adenocarcinoma SGC-7901 cells, lung adenocarcinoma A549 cells and fibrosarcoma HT-1080 cells. Moreover, to evaluate selectivity of compounds between cancer cell lines and non-cancer cell lines, fibroblasts L929 cells were also tested. As we expected, compound **32** and **33**, both had a low proportion of "bent" conformation, showed low activity against three cell lines. In contrast, compound **34**, which preferred "bent" conformation, showed much higher activity than **32** and **33**, and 4–37 fold lower activity in comparison to that **5**. (Table 3). Interestingly, although the potency of compound **34** is lower than colchicine and CA-4, it showed a higher selectivity between the tested cancer cell lines and non-cancer cell lines.

#### 2.5.2. Tubulin polymerization assay

To directly compare the inhibitory ability of tubulin polymerization, the effects of **33** and **34** on the tubulin polymerization were investigated *in vitro* (Fig. 7). **34** caused a dose-dependent inhibition

**Table 2**
Energy difference between the two conformations of designed compounds.

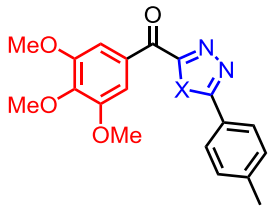


**32**, X = O
**33**, X = S
**34**, X = NH

| | E("bent")-E("straight") (kJ/mol) | Proportion of "bent" conformation |
|---|---|---|
| **32** | 20.19 | <0.1% |
| **33** | 29.70 | <0.1% |
| **34** | −31.66 | >99.9% |

of tubulin assembly with an $IC_{50}$ value of 7.71 μM, while **33** showed almost no effect on tubulin polymerization. These results unambiguously proved that **34** (with dominate "bent" conformation) has superior potency to binding with tubulin than **33** (with dominate "straight" conformation).

## 3. Conclusion

In this study, the B-ring caused conformational impacts on the bioactivities of SMART analogues, which were revealed for the first time through a series of calculations. Molecular modeling studies established the binding modes, which could satisfy all reported SMART analogues, and suggested that "bent" conformation was a preferred conformation for binding. DFT computations for the reported compounds confirmed that most of the active compounds had a considerable proportion of "bent" conformation. In addition, the introduction of the intramolecular hydrogen bond, steric effect and the fused heterocyclic scaffold strategy involved B-ring could improve the proportion of "bent" conformation or absolutely keep the "bent" conformation of the molecule. The conformational impact was validated through the designed and synthesized compounds. Furthermore, compound **34** displayed potent bioactivity against three types of human cancer cell lines and in tubulin polymerization assay.

As previously stated, the A-ring (TMP) and C-ring are crucial for optimal activity, and the spatial relationships of the two pharmacophores could be adjusted through the conjugated B-ring. In our study, we disclosed the "bent" conformational preference of the

**Table 3**
Bioactivity of the designed compounds.

| | Bioactivity against cell line, $IC_{50}$ (μM) | | | | Selectivity index[a] | Tubulin assembly activity, $IC_{50}$ (μM) |
|---|---|---|---|---|---|---|
| | SGC-7901 | A549 | HT-1080 | L929 | | |
| **32** | 6.77 ± 0.51 | 15.3 ± 0.9 | >100 | – | – | – |
| **33** | >100 | 35.3 ± 1.5 | >100 | – | – | >100 |
| **34** | 0.38 ± 0.02 | 1.07 ± 0.08 | 0.65 ± 0.03 | 42.6 ± 0.9 | 112.1 (SGC-7901)<br>39.8 (A549)<br>65.5 (HT-1080) | 7.71 |
| **1** | 0.134 ± 0.004 | 0.137 ± 0.006 | 0.042 ± 0.002 | 1.01 ± 0.08 | 7.5 (SGC-7901)<br>7.4 (A549)<br>24.0 (HT-1080) | – |
| **2** | 0.012 ± 0.003 | 0.016 ± 0.002 | 0.016 ± 0.006 | 0.82 ± 0.07 | 68.3 (SGC-7901)<br>51.3 (A549)<br>51.3 (HT-1080) | 0.64 |
| **5** | 0.019 ± 0.008 | 0.029 ± 0.009 | 0.15 ± 0.05 | – | – | 4.23 |

[a] Selectivity indexes were calculated by $IC_{50}$(L929)/$IC_{50}$(SGC-7901), $IC_{50}$(L929)/$IC_{50}$(A549) and $IC_{50}$(L929)/$IC_{50}$(HT-1080), respectively.

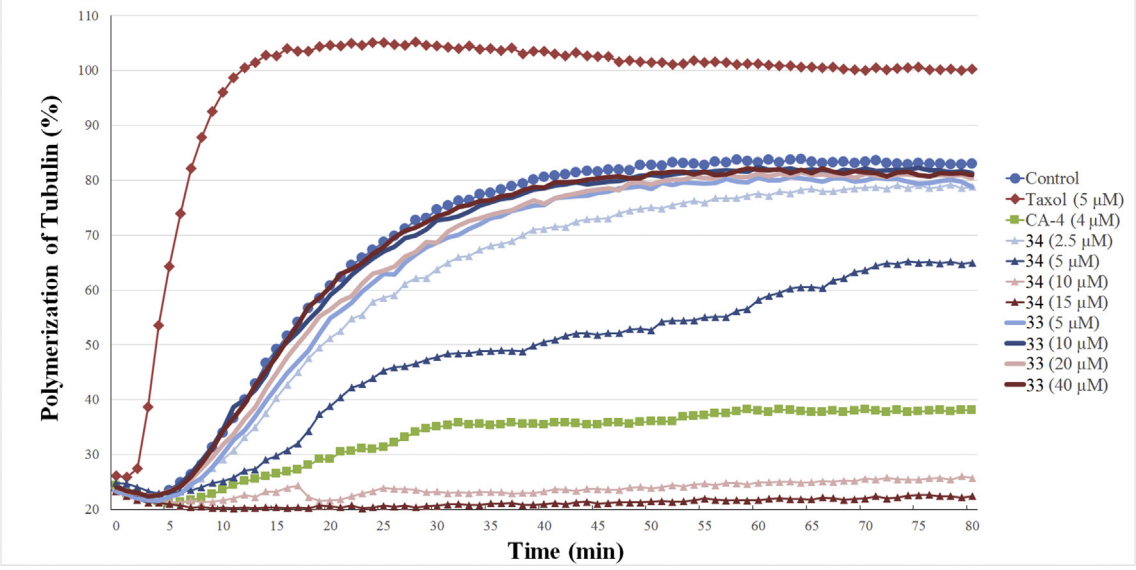


**Fig. 7.** Effects of **33** and **34** on tubulin polymerization. Tubulin had been pre-incubated for 1 min with **33** and **34** at various concentrations, CA-4 at 4 μM, Taxol at 5 μM or vehicle DMSO.

active SMART analogues through the review and analysis of data from other research groups and our own study. This work will inspire people to consider the importance of conformational preference in the design of novel SMART analogues. Further evaluation and optimization of **34** and several series of novel compounds with potent bioactivity discovered by the same strategy are currently in progress.

## 4. Materials and methods

### 4.1. Computations

#### 4.1.1. Molecular modeling studies

The molecular docking was carried out on Discovery Studio 3.5 software by CDOCKER program, and all PDB files were downloaded from the website of RCSB Protein Data Bank (http://www.rcsb.org/). The ligands were prepared by Avogadro [37] (Version 1.20) and optimized by molecular dynamic forcefield MMFF94 [38–42]. In particular, for the ligands with tautomerism, all tautomers were calculated by DFT computations (see *DFT computations*), and the tautomer with the lowest energy was selected for studies. Furthermore, The AlogP value of **1**, **5**~**31** were also calculated on Discovery Studio 3.5 software. The docking images shown in this paper were possessed by Discovery Studio 4.5 Visualizer.

MD simulation was carried out on Gromacs (Version 2016.4). GROMOS96 43a1 force field was used for the docked complex between tubulin (PDB code: 5LYJ) and **5** (including a GTP and a $Mg^{2+}$ nearby binding site). The coordinates of the top-rank pose of **5** and native GTP molecule were submitted to the PRODRG site (http://davapc1.bioch.dundee.ac.uk/cgi-bin/prodrg) and the initial geometries and topologies were retrieved. A cubic box with the periodic boundary conditions (PBC) was applied on the system. The simple point charge (SPC) water molecules were employed and 33 negative charges were added by replacing water molecules to ensure the overall charge neutrality of the simulated system. Each system was firstly energy minimized using the steepest descent method. Then, position restraint procedure was performed in association with 200-ps NVT (constant-temperature, constant-volume) and 200-ps NPT (constant-temperature, constant-pressure) ensembles. Finally, a 25-ns MD simulation was performed. The output trajectories were recorded every 2 ps for the purpose of subsequent analysis.

#### 4.1.2. DFT computations

The "bent" conformations of SMART analogues came from molecular docking poses in 5LYJ. The "straight" conformations were obtained by the manually modified bond angle between carbonyl and B-ring and further optimized by molecular dynamic forcefield MMFF94. All molecules were fully optimized by DFT basic set B3LYP/6-31G(d) on Gaussian 09 [43]. The result of optimization showed the energy of both two conformations for all molecules. The raw data with unit a.u. was transformed to kJ/mol (1 a.u. = 2625.5 kJ/mol) as shown in Tables 1 and 2.

Thermodynamic equilibrium was calculated according to the following formulas, and the results were also given on Tables 1 and 2.

$$\Delta G \approx E(bent) - E(straight) = -RTlnK$$

Here, E(bent) and E(straight) are come from DFT computations, R and T are constant,

$$R = 8.314\, J \cdot mol^{-1} \cdot K^{-1}, \quad T = 300K$$

Thus, equilibrium constant K could obtain, and

$$K = \frac{[bent]}{[straight]} = \frac{n(bent)}{n(straight)}$$

Here, [bent] and [straight] are the concentration of each conformation, n(bent) and n(straight) are amount of each conformation. Thus,

$$\textit{Estimated proportion of "bent" conformation} = \frac{n(bent)}{n(straight) + n(bent)} = \frac{K}{K+1}$$

### 4.2. Chemistry

#### 4.2.1. Reagents and equipment

All the solvents and chemical materials were commercially available and were used without further purification. Silica gel H (200–300 mesh) from Qingdao Haiyang Chemical Company was used for column chromatography. $^1H$ and $^{13}C$ NMR spectra were recorded in $CDCl_3$ or DMSO-$d_6$ (TMS as internal standard) using a Bruker Avance 600 spectrometers ($^1H$ at 600 MHz, $^{13}C$ at 150 MHz). Chemical shifts $\delta$ are in ppm, and the following abbreviations are used: singlet (s), doublet (d), triplet (t), multiplet (m), broad singlet (brs). Mass spectra (MS) were determined on an Agilent 1100-sl mass spectrometer (ESI) from Agilent Co., Ltd. HPLC (HPLC-LC-20AT, Shimadzu) using SPD-20A UV as the detector (UV light at 254 nm), C18 (4.6 x 250 mm, 0.45 mm) as HPLC analysis column.

#### 4.2.2. Synthetic procedures for 2-(3,4,5-trimethoxyphenyl) acetohydrazide (**36**)

To a solution of methyl 2-(3,4,5-trimethoxyphenyl)acetate (**35**, 1201 mg, 5 mmol) in methanol (30 mL), 80% hydrazine hydrate (0.78 mL, 12.5 mmol) was added. The reaction was monitored by TLC, and the mixture was concentrated under reduced pressure after 2 h. The crude product was purified by flash column chromatography (silica gel, DCM/MeOH, 50/1 to 20/1) to give the pure product as a white solid in 91% yield.

#### 4.2.3. Synthetic procedures for 4-methyl-N'-(2-(3,4,5-trimethoxyphenyl)acetyl)benzohydrazide (**37**)

To a suspended of **36** (1201 mg, 5 mmol) in toluene (20 mL), 4-methylbenzoyl chloride (773 mg, 5 mmol) in toluene (10 mL) was added under nitrogen. The reaction mixture was heated to reflux for 1 h and was concentrated under reduced pressure. The crude products were used in next step without further purification.

#### 4.2.4. Synthetic procedures for 2-(4-methylphenyl)-5-(3,4,5-trimethoxybenzyl)-1,3,4-oxadiazole (**38**)

A mixture of **37** (358 mg, 1 mmol), the $K_2CO_3$ (415 mg, 3 mmol) and TsCl (286 mg, 1.5 mmol) in the acetone (10 mL) was stirred at 40 °C for 4 h. Then, 60 mL water was added, and the mixture was extracted with EtOAc. Then the combined organic layers were washed with brine, dried, filtered, and concentrated. The resultant residue was purified by flash column chromatography (silica gel, PE/EA, 10/1 to 4/1) to afford the desired product **38** (yield: 85%) as a white soild. $^1H$ NMR (600 MHz, $CDCl_3$) $\delta$ 7.89 (2H, d, $J$ = 8.2 Hz), 7.28 (2H, d, $J$ = 8.0 Hz), 6.57 (2H, s), 4.19 (2H, s), 3.85 (6H, s), 3.82 (3H, s), 2.40 (3H, s); $^{13}C$ NMR (150 MHz, $CDCl_3$) $\delta$ 165.29, 164.85, 153.45, 142.18, 137.33, 129.66, 129.43, 126.72, 121.02, 105.83, 60.79, 56.12, 32.09, 21.56. MS (ESI) $m/z$ 341.1 $[M+H]^+$, 363.1 $[M+Na]^+$.

#### 4.2.5. Synthetic procedures for 2-(4-methylphenyl)-5-(3,4,5-trimethoxybenzyl)-1,3,4- thiadiazole (**39**)

A mixture of **37** (358 mg, 1 mmol) and Lawesson reagent (809 mg, 2 mmol) in toluene (20 mL) was allow to reflux for 1 h. Then, the mixture was filtered and concentrated. The resultant residue was purified by flash column chromatography (silica gel, PE/EA, 10/1 to 4/1) to afford the desired product **39** (yield: 70%) as a yellow soild. $^1$H NMR (600 MHz, $CDCl_3$) $\delta$ 7.77 (2H, d, $J = 8.0$ Hz), 7.27 (2H, d, $J = 8.0$ Hz), 6.54 (2H, s), 4.34 (2H, s), 3.82 (6H, s), 3.81 (3H, s), 2.36 (3H, s); $^{13}$C NMR (150 MHz, $CDCl_3$) $\delta$ 169.36, 169.08, 153.46, 141.36, 137.19, 132.70, 129.67, 127.61, 127.33, 105.72, 60.75, 56.07, 36.76, 21.35. MS (ESI) *m/z* 357.1 $[M+H]^+$, 379.1 $[M+Na]^+$.

#### 4.2.6. Synthetic procedures for 3-(4-methylphenyl)-5-(3,4,5-trimethoxybenzyl)-4H-1,2,4-triazole (**41**)

A mixture of 2-(3,4,5-trimethoxyphenyl)acetonitrile (**40**, 414 mg, 2 mmol), 4-methylbenzohydrazide (300 mg, 2 mmol) and $K_2CO_3$ (415 mg, 3 mmol) in *n*-BuOH (15 mL) was stirred under microwave irradiation (150 °C, 25 min). Then, 25 mL water was added, and the mixture was extracted with EtOAc. The combined organic layers were then washed with brine, dried, filtered, and concentrated. The resultant residue was purified by flash column chromatography (silica gel, PE/EA, 6/1 to 2/1) to afford the desired product **41** (yield: 72%) as a white soild.$^1$H NMR (600 MHz, $CDCl_3$) $\delta$ 7.83 (2H, d, $J = 8.1$ Hz), 7.13 (2H, d, $J = 8.0$ Hz), 6.45 (2H, s), 4.01 (2H, s), 3.73 (3H, s), 3.67 (6H, s), 2.32 (3H, s); $^{13}$C NMR (150 MHz, $CDCl_3$) $\delta$ 167.72, 159.20, 152.97, 139.68, 132.26, 129.29, 128.66, 127.28, 126.14, 105.53, 60.59, 57.93, 33.77, 21.21. MS (ESI) *m/z* 340.1 $[M+H]^+$, 362.1 $[M+Na]^+$, 338.1 $[M-H]^-$.

#### 4.2.7. General synthetic procedures for designed compounds (**32**, **33** and **34**)

To a solution of the corresponding reactant (**38**, **39** or **41**, 1 mmol) in acetone (10 mL), $KMnO_4$ (316 mg, 2 mmol) was added. The mixture was stirred at room temperature for 2–6 h. The reaction was monitored by TLC. After completion, the mixture was filtered and concentrated. The resultant residue was purified by PTLC to afford the desired product.

*(5-(4-methylphenyl)-1,3,4-oxadiazol*-2-yl*)(3,4,5-trimethoxyphenyl)methanone* (**32**). White solid, yield: 43%; HPLC Purity: 98.7%. $^1$H NMR (600 MHz, $CDCl_3$) $\delta$ 8.11 (2H, d, $J = 12.1$ Hz), 7.97 (2H, s), 7.37 (2H, d, $J = 12.1$ Hz), 3.99 (3H, s), 3.98 (6H, s), 2.46 (3H, s); $^{13}$C NMR (150 MHz, $CDCl_3$) $\delta$ 175.94, 166.05, 160.91, 153.03, 144.26, 143.69, 130.88, 129.97, 129.11, 127.72, 108.40, 61.06, 56.32, 21.75. HRMS calcd for $C_{19}H_{19}N_2O_5^+$ $[M+H]^+$ 355.1288, found 355.1304.

*(5-(4-methylphenyl)-1,3,4-thiadiazol*-2-yl*)(3,4,5-trimethoxyphenyl)methanone* (**33**). Yellow solid, yield: 61%; HPLC Purity: 97.9%. $^1$H NMR (600 MHz, $CDCl_3$) $\delta$ 8.00 (2H, s), 7.97 (2H, d, $J = 12.2$ Hz), 7.33 (2H, d, $J = 12.1$ Hz), 3.99 (3H, s), 3.98 (6H, s), 2.44 (3H, s); $^{13}$C NMR (150 MHz, $CDCl_3$) $\delta$ 181.40, 172.75, 169.22, 152.94, 143.88, 142.88, 130.07, 129.26, 128.27, 126.71, 108.80, 61.03, 56.31, 21.59. HRMS calcd for $C_{19}H_{19}N_2O_4S^+$ $[M+H]^+$ 371.1060, found 371.1080.

*(3-(4-methylphenyl)-1H-1,2,4-triazol*-5-yl*)(3,4,5-trimethoxyphenyl)methanone* (**34**). White solid, yield: 66%; HPLC Purity: 97.0%. $^1$H NMR (600 MHz, $CDCl_3$) $\delta$ 8.10 (2H, s), 8.04 (2H, d, $J = 11.6$ Hz), 7.29 (2H, d, $J = 11.5$ Hz), 3.98 (9H, s), 2.41 (3H, s); $^{13}$C NMR (150 MHz, $CDCl_3$) $\delta$ 180.90, 160.84, 155.17, 152.78, 143.59, 140.36, 129.96, 129.53, 126.47, 126.36, 108.75, 60.99, 56.17, 21.41. HRMS calcd for $C_{19}H_{20}N_3O_4^+$ $[M+H]^+$ 354.1448, found 354.1482, calcd for $C_{19}H_{19}N_3O_4^-$ $[M-H]^-$ 352.1303, found 352.1334.

### 4.3. Biology

#### 4.3.1. MTT assay

MTT assays were used to measure the cell viability after treatment. Briefly, 4–10 × $10^3$ cells/well were seeded in 96-well plates (Corning, NY, USA), cultured for 24 h, and treated with various concentrations of compounds for 72 h or incubated with SNP (10 mM) or Haemoglobin (10 mM) for 2 h. Then, it was treated with **5**, **32**, **33** or **34** (in different concentrates) for the indicated times. The DMSO concentration was kept below 0.05% in cell culture so it did not affect on cell growth. Then, MTT solution (5 mg/mL in PBS) was added (20 mL/well) to each well and incubated for another 4 h at 37 °C. The purple formazan crystals were dissolved in 100 mL dimethyl sulfoxide, and the plates were read on a plate reader (MK3, Thermo, German) at 492 nm. Experiments were repeated three times.

#### 4.3.2. Tubulin polymerization assay

In vitro tubulin polymerization assays were conducted as described in the manufacturer's protocol (Cytoskeleton, Cat.#BK011P) using 96-well plates. Briefly, **33**, **34**, CA-4 or Taxol were incubated with purified porcine tubulin (2 mg/mL) and buffer containing 10% glycerol and 1 mM GTP at 37 °C, and the effects of these compounds on tubulin polymerization were monitored kinetically for 82 min using a plate reader (Biotek Synergy HT, Winoo-skin, VT, USA). The increase in the relative fluorescence unit (RFU) was measured at an excitation of 340 ± 20 nm and emission of 415 ± 20 nm every minute. Experiments were repeated three times.

## Author contributions

Y.W., Q.G., D.Z, P.Y., D.F. and J.D. performed the experiments. D.Z, K.B. and W.Z. analyzed, interpreted the data and wrote the paper.

## Notes

The authors declare no competing financial interest.

## Acknowledgements

We gratefully acknowledge the National Natural Science Foundation of China (81673293, 81602969, 30973614), the Doctoral Research Funding of Liaoning Province (201601144), the Education Fund Item of Liaoning Province (201610163L12), the Science and Technology Research Project of Education Department of Liaoning Province (201610163L10), Liaoning Province Undergraduate Training Program for Innovation (201610163019) and the Shenyang Science & Technology Bureau Item (F12-277-1-23, F17-231-1-42) for generous financial support. This work was also supported by Support Program for the Career Development of Junior Faculty of Shenyang Pharmaceutical University.

## Appendix A. Supplementary data

Supplementary data to this article can be found online at https://doi.org/10.1016/j.ejmech.2018.09.045.

## References

[1] M.J. Perez-Perez, E.M. Priego, O. Bueno, M.S. Martins, M.D. Canela, S. Liekens, Blocking blood flow to solid tumors by destabilizing tubulin: an approach to targeting tumor growth, J. Med. Chem. 59 (2016) 8685–8711.
[2] M.A. Jordan, L. Wilson, Microtubules as a target for anticancer drugs, Nat. Rev. Canc. 4 (2004) 253–265.
[3] Y. Lu, J. Chen, M. Xiao, W. Li, D.D. Miller, An overview of tubulin inhibitors that

interact with the colchicine binding site, Pharm. Res. (N. Y.) 29 (2012) 2943–2971.
[4] A. Massarotti, A. Coluccia, R. Silvestri, G. Sorba, A. Brancale, The tubulin colchicine domain: a molecular modeling perspective, ChemMedChem 7 (2012) 33–42.
[5] Y. Lu, C.M. Li, Z. Wang, C.R. Ross 2nd, J. Chen, J.T. Dalton, W. Li, D.D. Miller, Discovery of 4-substituted methoxybenzoyl-aryl-thiazole as novel anticancer agents: synthesis, biological evaluation, and structure-activity relationships, J. Med. Chem. 52 (2009) 1701–1711.
[6] J. Chen, Z. Wang, C.M. Li, Y. Lu, P.K. Vaddady, B. Meibohm, J.T. Dalton, D.D. Miller, W. Li, Discovery of novel 2-aryl-4-benzoyl-imidazoles targeting the colchicines binding site in tubulin as potential anticancer agents, J. Med. Chem. 53 (2010) 7414–7427.
[7] M. Xiao, S. Ahn, J. Wang, J. Chen, D.D. Miller, J.T. Dalton, W. Li, Discovery of 4-Aryl-2-benzoyl-imidazoles as tubulin polymerization inhibitor with potent antiproliferative properties, J. Med. Chem. 56 (2013) 3318–3329.
[8] G. La Regina, R. Bai, A. Coluccia, V. Famiglini, S. Pelliccia, S. Passacantilli, C. Mazzoccoli, V. Ruggieri, L. Sisinni, A. Bolognesi, W.M. Rensen, A. Miele, M. Nalli, R. Alfonsi, L. Di Marcotullio, A. Gulino, A. Brancale, E. Novellino, G. Dondio, S. Vultaggio, M. Varasi, C. Mercurio, E. Hamel, P. Lavia, R. Silvestri, New pyrrole derivatives with potent tubulin polymerization inhibiting activity as anticancer agents including hedgehog-dependent cancer, J. Med. Chem. 57 (2014) 6531–6552.
[9] D.J. Feng, Y. Wu, H. Wang, Z.S. Bai, D.F. Wang, D.Y. Zuo, K. Bao, Y.L. Wu, W.G. Zhang, Synthesis and antiproliferative activity of 2-aryl-4-(3,4,5-trimethoxybenzoyl)-1,2,3-triazol derivatives as microtubule-destabilizing agents, RSC Adv. 7 (2017) 29103–29111.
[10] Z. Bai, M. Gao, H. Zhang, Q. Guan, J. Xu, Y. Li, H. Qi, Z. Li, D. Zuo, W. Zhang, Y. Wu, BZML, a novel colchicine binding site inhibitor, overcomes multidrug resistance in A549/Taxol cells by inhibiting P-gp function and inducing mitotic catastrophe, Canc. Lett. 402 (2017) 81–92.
[11] R. Romagnoli, P.G. Baraldi, M.D. Carrion, C.L. Cara, O. Cruz-Lopez, D. Preti, M. Tolomeo, S. Grimaudo, A. Di Cristina, N. Zonta, J. Balzarini, A. Brancale, T. Sarkar, E. Hamel, Design, synthesis, and biological evaluation of thiophene analogues of chalcones, Bioorg. Med. Chem. 16 (2008) 5367–5376.
[12] R. Romagnoli, P.G. Baraldi, V. Remusat, M.D. Carrion, C.L. Cara, D. Preti, F. Fruttarolo, M.G. Pavani, M.A. Tabrizi, M. Tolomeo, S. Grimaudo, J. Balzarini, M.A. Jordan, E. Hamel, Synthesis and biological evaluation of 2-(3',4',5'-trimethoxybenzoyl)-3-amino 5-aryl thiophenes as a new class of tubulin inhibitors, J. Med. Chem. 49 (2006) 6425–6428.
[13] R. Romagnoli, P.G. Baraldi, M.G. Pavani, M.A. Tabrizi, D. Preti, F. Fruttarolo, L. Piccagli, M.K. Jung, E. Hamel, M. Borgatti, R. Gambari, Synthesis and biological evaluation of 2-amino-3-(3',4',5'-trimethoxybenzoyl)-5-aryl thiophenes as a new class of potent antitubulin agents, J. Med. Chem. 49 (2006) 3906–3915.
[14] R. Romagnoli, P.G. Baraldi, M.K. Salvador, D. Preti, M. Aghazadeh Tabrizi, A. Brancale, X.H. Fu, J. Li, S.Z. Zhang, E. Hamel, R. Bortolozzi, E. Porcu, G. Basso, G. Viola, Discovery and optimization of a series of 2-aryl-4-amino-5-(3',4',5'-trimethoxybenzoyl)thiazoles as novel anticancer agents, J. Med. Chem. 55 (2012) 5433–5445.
[15] Y. Lu, C.M. Li, Z. Wang, J. Chen, M.L. Mohler, W. Li, J.T. Dalton, D.D. Miller, Design, synthesis, and SAR studies of 4-substituted methoxylbenzoyl-aryl-thiazoles analogues as potent and orally bioavailable anticancer agents, J. Med. Chem. 54 (2011) 4678–4693.
[16] Q. Guan, D.J. Feng, Z.S. Bai, Y.H. Cui, D.Y. Zuo, M.A. Zhai, X.W. Jiang, W.B. Zhou, K. Bao, Y.L. Wu, W.G. Zhang, Microwave-assisted synthesis, molecular docking and antiproliferative activity of (3/5-aryl-1,2,4-oxadiazole-5/3-yl)(3,4,5-trimethoxyphenyl)methanone oxime derivatives, Med. Chem. Commun. 6 (2015) 1484–1493.
[17] O. Mesenzani, A. Massarotti, M. Giustiniano, T. Pirali, V. Bevilacqua, A. Caldarelli, P. Canonico, G. Sorba, E. Novellino, A.A. Genazzani, G.C. Tron, Replacement of the double bond of antitubulin chalcones with triazoles and tetrazoles: synthesis and biological evaluation, Bioorg. Med. Chem. Lett 21 (2011) 764–768.
[18] M. Dong, F. Liu, H. Zhou, S. Zhai, B. Yan, Novel natural product- and privileged scaffold-based tubulin inhibitors targeting the colchicine binding site, Molecules 21 (2016) 1375.
[19] R.B. Ravelli, B. Gigant, P.A. Curmi, I. Jourdain, S. Lachkar, A. Sobel, M. Knossow, Insight into tubulin regulation from a complex with colchicine and a stathmin-like domain, Nature 428 (2004) 198–202.
[20] F.M. Ranaivoson, B. Gigant, S. Berritt, M. Joullie, M. Knossow, Structural plasticity of tubulin assembly probed by vinca-domain ligands, Acta Crystallogr. D Biol. Crystallogr. 68 (2012) 927–934.
[21] A.E. Prota, F. Danel, F. Bachmann, K. Bargsten, R.M. Buey, J. Pohlmann, S. Reinelt, H. Lane, M.O. Steinmetz, The novel microtubule-destabilizing drug BAL27862 binds to the colchicine site of tubulin with distinct effects on microtubule organization, J. Mol. Biol. 426 (2014) 1848–1860.
[22] R. Gaspari, A.E. Prota, K. Bargsten, A. Cavalli, M.O. Steinmetz, Structural basis of cis- and trans-combretastatin binding to tubulin, Inside Chem. 2 (2017) 102–113.
[23] P. Zhou, Y. Liu, L. Zhou, K. Zhu, K. Feng, H. Zhang, Y. Liang, H. Jiang, C. Luo, M. Liu, Y. Wang, Potent antitumor activities and structure basis of the chiral beta-lactam bridged analogue of combretastatin A-4 binding to tubulin, J. Med. Chem. 59 (2016) 10329–10334.
[24] M.D. Canela, S. Noppen, O. Bueno, A.E. Prota, K. Bargsten, G. Saez-Calvo, M.L. Jimeno, M. Benkheil, D. Ribatti, S. Velazquez, M.J. Camarasa, J.F. Diaz, M.O. Steinmetz, E.M. Priego, M.J. Perez-Perez, S. Liekens, Antivascular and antitumor properties of the tubulin-binding chalcone TUB091, Oncotarget 8 (2017) 14325–14342.
[25] N. Fani, A.K. Bordbar, Y. Ghayeb, S. Sepehri, Integrating docking and molecular dynamics approaches for a series of proline-based 2,5-diketopiperazines as novel alphabeta-tubulin inhibitors, J. Biomol. Struct. Dyn. 33 (2015) 2285–2295.
[26] A.K. Ghose, V.N. Viswanadhan, J.J. Wendoloski, Prediction of hydrophobic (lipophilic) properties of small organic molecules using fragmental methods: an analysis of ALOGP and CLOGP methods, J. Phys. Chem. 102 (1998) 3762–3772.
[27] J. Jiang, C. Zheng, K. Zhu, J. Liu, N. Sun, C. Wang, H. Jiang, J. Zhu, C. Luo, Y. Zhou, Quantum chemistry calculation-aided structural optimization of combretastatin A-4-like tubulin polymerization inhibitors: improved stability and biological activity, J. Med. Chem. 58 (2015) 2538–2546.
[28] Y. Lu, J. Chen, J. Wang, C.M. Li, S. Ahn, C.M. Barrett, J.T. Dalton, W. Li, D.D. Miller, Design, synthesis, and biological evaluation of stable colchicine binding site tubulin inhibitors as potential anticancer agents, J. Med. Chem. 57 (2014) 7355–7366.
[29] D.J. Hwang, J. Wang, W. Li, D.D. Miller, Structural optimization of indole derivatives acting at colchicine binding site as potential anticancer agents, ACS Med. Chem. Lett. 6 (2015) 993–997.
[30] K.E. Arnst, Y. Wang, D.J. Hwang, Y. Xue, T. Costello, D. Hamilton, Q. Chen, J. Yang, F. Park, J.T. Dalton, D.D. Miller, W. Li, A potent, metabolically stable tubulin inhibitor targets the colchicine binding site and overcomes taxane resistance, Canc. Res. 78 (2018) 265–277.
[31] Q. Xu, Y. Wang, J. Xu, M. Sun, H. Tian, D. Zuo, Q. Guan, K. Bao, Y. Wu, W. Zhang, Synthesis and bioevaluation of 3,6-Diaryl-[1,2,4]triazolo[4,3-b] pyridazines as antitubulin agents, ACS Med. Chem. Lett. 7 (2016) 1202–1206.
[32] Q. Xu, M. Sun, Z. Bai, Y. Wang, Y. Wu, H. Tian, D. Zuo, Q. Guan, K. Bao, Y. Wu, W. Zhang, Design, synthesis and bioevaluation of antitubulin agents carrying diaryl-5,5-fused-heterocycle scaffold, Eur. J. Med. Chem. 139 (2017) 242–249.
[33] Q. Xu, K. Bao, M. Sun, J. Xu, Y. Wang, H. Tian, D. Zuo, Q. Guan, Y. Wu, W. Zhang, Design, synthesis and structure-activity relationship of 3,6-diaryl-7H-[1,2,4] triazolo[3,4-b][1,3,4]thiadiazines as novel tubulin inhibitors, Sci. Rep. 7 (2017) 11997.
[34] P. Stabile, A. Lamonica, A. Ribecai, D. Castoldi, G. Guercio, O. Curcuruto, Mild and convenient one-pot synthesis of 1,3,4-oxadiazoles, Tetrahedron Lett. 51 (2010) 4801–4805.
[35] B. Gierczyk, M. Zalas, Synthesis of substituted 1,3,4-thiadiazoles using Lawesson's reagent, Org. Prep. Proced. Int. 37 (2005) 213–222.
[36] K.S. Yeung, M.E. Farkas, J.F. Kadow, N.A. Meanwell, A base-catalyzed, direct synthesis of 3,5-disubstituted 1,2,4-triazoles from nitriles and hydrazides, Tetrahedron Lett. 46 (2005) 3429–3432.
[37] M.D. Hanwell, D.E. Curtis, D.C. Lonie, T. Vandermeersch, E. Zurek, G.R. Hutchison, Avogadro: an advanced semantic chemical editor, visualization, and analysis platform, J. Cheminf. 4 (2012) 17.
[38] T.A. Halgren, Merck molecular force field. I. Basis, form, scope, parameterization, and performance of MMFF94, J. Comput. Chem. 17 (1996) 490–519.
[39] T.A. Halgren, Merck molecular force field. II. MMFF94 van der Waals and electrostatic parameters for intermolecular interactions, J. Comput. Chem. 17 (1996) 520–552.
[40] T.A. Halgren, Merck molecular force field. III. Molecular geometries and vibrational frequencies for MMFF94, J. Comput. Chem. 17 (1996) 553–586.
[41] T.A. Halgren, R.B. Nachbar, Merck molecular force field. IV. conformational energies and geometries for MMFF94, J. Comput. Chem. 17 (1996) 587–615.
[42] T.A. Halgren, Merck molecular force field. V. Extension of MMFF94 using experimental data, additional computational data, and empirical rules, J. Comput. Chem. 17 (1996) 616–641.
[43] M.J. Frisch, G.W. Trucks, H.B. Schlegel, G.E. Scuseria, M.A. Robb, J.R. Cheeseman, G. Scalmani, V. Barone, B. Mennucci, G.A. Petersson, H. Nakatsuji, M. Caricato, X. Li, H.P. Hratchian, A.F. Izmaylov, J. Bloino, G. Zheng, J.L. Sonnenberg, M. Hada, M. Ehara, K. Toyota, R. Fukuda, J. Hasegawa, M. Ishida, T. Nakajima, Y. Honda, O. Kitao, H. Nakai, T. Vreven, J.A. Montgomery, J E.P Jr, F. Ogliaro, M. Bearpark, J.J. Heyd, E. Brothers, K.N. Kudin, V.N. Staroverov, R. Kobayashi, J. Normand, K. Raghavachari, A. Rendell, J.C. Burant, S.S. Iyengar, J. Tomasi, M. Cossi, N. Rega, J.M. Millam, M. Klene, J.E. Knox, J.B. Cross, V. Bakken, C. Adamo, J. Jaramillo, R. Gomperts, R.E. Stratmann, O. Yazyev, A.J. Austin, R. Cammi, C. Pomelli, J.W. Ochterski, R.L. Martin, K. Morokuma, V.G. Zakrzewski, G.A. Voth, P. Salvador, J.J. Dannenberg, S. Dapprich, A.D. Daniels, Ö. Farkas, J.B. Foresman, J.V. Ortiz, J. Cioslowski, a.D.J. Fox, Gaussian 09, Gaussian, Inc., Wallingford CT, 2009.